Analysis of the performance of a Thoracoscapular Shoulder Model

T.A. Ruiter

Delft University of Technology

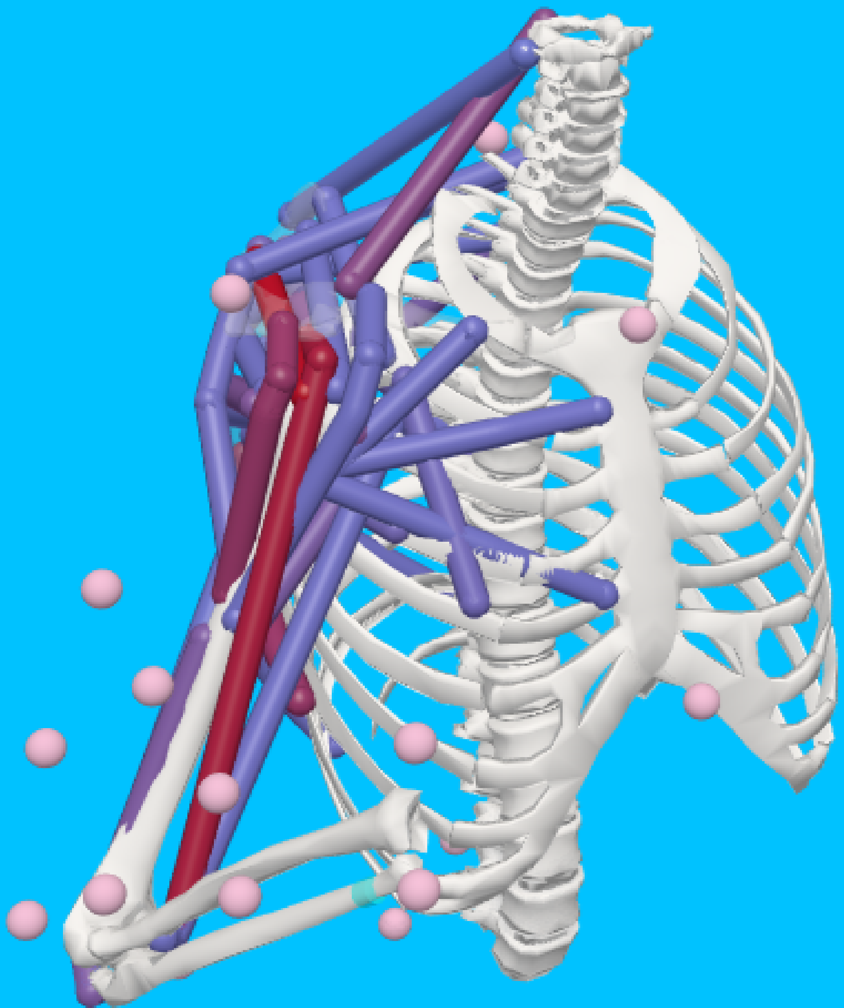

TU Delft

Analysis of the performance of a Thoracoscapular Shoulder Model

by

T.A. Ruiter

to obtain the degree of Master of Science
at the Delft University of Technology,
to be defended publicly on the 24th of January 2025 at 12:45 PM.

Student number:	4912373	
Project duration:	January 1, 2024 – January 24, 2025	
Thesis committee:	AP. dr. ir. A. Seth,	TU Delft, supervisor
	Dr. ir. I. Belli,	TU Delft
	AP. dr. ir. L. Peternel	TU Delft

An electronic version of this thesis is available at `http://repository.tudelft.nl/`.

TU Delft

Preface

A lot can happen in one year. Last year I worked on this thesis and I learned a lot about biomechanics, musculoskeletal modeling and OpenSim. The PTbot project is a great example of how these tools can be put into practice and I am glad to have finished my study career on this project. I want to thank Ajay Seth for connecting me to this project and being my supervisor to this project. With your knowledge about biomechanics you helped me a lot during my thesis by giving valuable feedback. I also want to thank the rest of the PTbot group; Italo Belli for always being there to help with big and small problems, Luka Peternel and Micah Prendergast for providing different views and Florian and Tom where I could talk about my daily struggles. The weekly PTbot meetings provided useful guidance throughout last year. I also want to thank the Computational Biomechanics Lab of the Faculty of Mechanical Engineering. There are a lot of interesting projects running. Giving weekly updates and hearing weekly updates from these projects helped staying motivated.

During my thesis I not only gained more technical skills, but also improved my soft skills. I learned that a research project has its ups and downs and how to tackle specific problems. I want to thank my study groups for the work and vent sessions.

Towards the end of this project I gained extra interest in rehabilitation. As I am currently recovering from an ACL reconstruction surgery, I found that it is difficult to determine how far you can push the rehabilitation exercises. The need for a PTbot became even clearer to me than I had wished for. This surgery made the last month even more hectic than the last month of a thesis project already is. I am very grateful to my parents and brother to help me with this surgery. Without this help, I wouldn't be able to defend my thesis on the 24th of January.

T.A. Ruiter
Delft, January 2025

Summary

Musculoskeletal modeling has the opportunity to improve the rehabilitation process after a shoulder injury by monitoring the muscle activations and tendon strain during rehabilitation exercises. The PT-bot project combines a robot arm and a Thoracoscapular Shoulder Model (TSM) in order to track the shoulder movement and give a physiotherapist insight on the what happens in a human body, but the performance of the TSM is not yet analyzed. This paper aims to get a better understanding of the TSM by testing its performance in a wide range of motion.

With an existing isometric dataset, the TSM is positioned in five different shoulder configurations. First, the model is scaled in four steps. With the help of the muscle moment arms an normalized fiber length of this scaled model, improvements have been made to the latissimus dorsi. This improved model is scaled a second time whereafter an RMR solver is run. This RMR solver computed the muscle activation levels and joint torque residuals of the TSM. The RMR solver is first run with experimental external forces applied on the hand, in order to validate the TSM by comparing the muscle activations to EMG data. After that, the RMR solver is run with artificial external forces, in order to understand which muscles are activated during push and pull exercises.

The Mean Average Error (MAE) between the muscle activation levels and experimental EMG measurements has been calculated for the validation of the TSM. They show that the TSM performs well when the shoulder planar elevation and shoulder elevation angles, but the performance decreases when these angles increase. The active fiber forces have been calculated and the muscles with the major contribution have been identified for pulling and pushing. The Infraspinatus, trapezius and deltoid play a major role for pushing exercises and the subscapularis, teres major and biceps for pulling exercises. The total muscle force needed for pushing is higher than for pulling.

Contents

Nomenclature

Abbreviations

Abbreviation	Definition
DSEM	Delft Elbow and Shoulder Model
EMG	Electromyography
IK	Inverse Kinematics
MMA	Muscle Moment Arm
MVC	Maximum Voluntary Contraction
RMR solver	Random Muscle Redundancy solver
RoM	Range of Motion

Symbols

Symbol	Definition	Unit
a	Muscle activation level	[-]
Hz	Hertz	[1/s]
e	Marker error	[mm]
t	Time	[s]
T	Torque	[Nm]
V	Velocity	[m/s]

Muscle abbreviations

Abbreviation	Muscle
Infra	Infraspinatus
Supra	Supraspinatus
PecMajorC	Clavicular pectoralis major
PecMajorS	Sternal pectoralis major
Lats	Latissimus dorsi
LatsS	Superior latissimus dorsi
LatsM	Middle latissimus dorsi
LatsI	Inferior latissimus dorsi
Sert	Serratus anterior
TrapLow	Inferior trapezius
TrapMid	Medial trapezius
TrapUp	Superior trapezius

1 Introduction

The rotator cuff consists of the infraspinatus, supraspinatus, subscapularis and teres minor. A tear in one of these muscles is the most common shoulder injury as one fifth to one third of the population experiences rotator cuff tears in their lifetime [1], [2], [3]. There are several treatment options. Physiotherapy plays an essential role in recovering shoulder functionality [4]. A big issue with rehabilitation is that there is no standard treatment for everyone and that it can last up to a year. Although excercises improve the recovering time, there is a big concern for damaging the recovering tissue, for example by putting too much strain on the rotator cuff [5], [6]. Currently, treatment is mostly based on clinical experience and not on scientific protocols [7]. Getting more information on what's happening during rehabilitation can allow the patient to do exercises with less risk of damaging the tissue.

The PTbot project [8] aims to tackle this problem by monitoring a patient's movement and muscle functioning by combining a robot arm and a musculoskeletal shoulder model. With the help of a robot arm, the shoulder movement of a patient can be tracked. A musculoskeletal shoulder model can be used to calculate the muscle activations and tendon strain. These activations and strain can help the patient with performing exercises, without damaging the recovering tissue.

1.1. Musculoskeletal modeling

Musculoskeletal modeling software, such as OpenSim [9] is a powerful tool for understanding the mechanics inside a human body. These models consists out of the skeleton and muscles. The skeleton is modeled as a rigid multi-body system, made up from the bones and joints. The joints are moved by activation of the muscles. The muscles are attached to the bones and the force produced by the muscles results in a torque around these joints. These torques results in a specific movement, similar to what happens in the human body [10]. With the help of inverse kinematics these steps can be reversed: from given motion data, the joint configurations of the human body can be calculated in a musculoskeletal model. From these joint configurations, muscle activations and forces can be calculated.

1.2. Verification & Validation

As a model is an estimation of reality, it should always be verified and validated in order to see whether the model's results are trustworthy. The verification process determines whether the implementation of a model corresponds to the conceptual description of the model: verification is needed to test if the biomechanics and mathematics are implemented correctly [11], [12], The validation process determines whether the model accurately represents the real world [11]. The validation process generally consists out of three parts: a comparison between the model and experimental results, extrapolating the model's prediction to its intended use and determining whether the accuracy is good enough for this intended use [13].

Surface EMG data is currently the standard to use for this comparison [10]. The main advantage of sEMG is that it is a cheap, noninvasive way to gather data about muscle recruitment under the skin. sEMG is however sensitive to crosstalk and the generated muscle force cannot be obtained with EMG measurements [13]. Nonetheless, comparing EMG patterns to a model's muscle activation patterns is useful to see if the model correctly predicts which muscles are recruited for different tasks.

The Muscle Moment Arm (MMA) is another common metric that can be used for validation. By comparing the MMA of the model to data from cadaveric studies, the muscle paths of the model can be validated. This makes MMA a useful metric to validate the musculoskeletal geometry of a model [12]. There are several cadaveric studies that have obtained MMA values, but they use different muscle bundles. This makes it hard to compare the MMA's of two different cadaveric studies [14].

Whether a model is properly validated, is partially dependent on the task [13]: the range of motion (RoM) of the experimental data should be similar to the RoM of the application of the model. Extrapolating the validation results to other model poses is dangerous, due to the complexity of a biomechanical model. Blind validation indicates that the experimental data used for validation is independent from the data used to construct the model. Blind validation ensures that the validation is more robust and the model is more reliable to use for other applications [13].

1.3. Thoracoscapular Shoulder model

A thoracoscapular shoulder model (TSM) [15] is used in the PTBot project for the simulations of the shoulder joint [16]. This model uses the bone geometries from Holzbaur [17], combined with muscle paths and architecture from Klein Breteler [18]. The muscles are bundled using muscle bundles from Van der Helm [19] and the paths are adjusted to match the MMA from Ackland [20]. The triceps brachii and biceps brachii muscles are adjusted to represent respectively three and two heads [21]. The TSM uses 35 muscle tendon elements that control 7 degrees of freedom.

The TSM is previously validated in different studies by comparing the muscle activations to EMG measurements. The muscle activations were compared to sEMG measurements by Seth et al. in 2019 [15] and by Belli et al. in 2023 [22]. During shrugging, flexion and abduction trials, the EMG values were recorded for 8 muscles and. The Mean Absolute Error (MAE) was calculated between the model's predicted muscle activations and sEMG values. For these trials, most muscles showed an MAE below 0.1, except for the trapezius superior, latissimus dorsi and teres major. In both researches, the latissimus dorsi performs worse than the other muscles. In 2024, the TSM is used by Santos Carvalho to research wheelchair propulsion [21]. The activation levels of five muscles were compared to sEMG measurements. The pectoralis major had the highest MAE during this research. There was no sEMG measurement of the latissimus dorsi, but the MMA was compared to a cadaveric study from Ackland et al. [20]. The MMA of the modeled latissimus dorsi have a maximum value at a lower shoulder elevation angle than the experimental data. The validation results of these three studies suggests that the modeling of the latissimus dorsi in the TSM can be improved.

The TSM is validated for flexion, abduction and shrugging tasks [15], [22] and wheelchair propulsion [21]. These movement have one or twee degrees of freedom, which makes it harder to extrapolate the validation results. During physical therapy, exercises can vary a lot. This results in the shoulder to move in a wide RoM and to exert forces in various direction. The EMG comparison results of these experiments cannot be extrapolated to be used for validating the TSM during these exercises. In order to acquire trustworthy results for the PTbot, the TSM model should therefore be validated more extensively.

1.4. Project aim

The aim of this paper is to get a better understanding of the performance of the TSM by testing it in a wider range of motion. This aim is achieved in three steps: verification of the TSM (step 1), validation of the TSM (step 2) and investigation of the muscle contributions (step 3). In the first step, the model is verified in different shoulder configurations using a dataset from a study of the University of Waterloo [23]. This dataset provides motion data, EMG data and external force data isometric trials in five different arm positions. The motion data has been used to set the model in different configurations. As previous research has shown that the moment arms of the latissimus dorsi can be improved, modifications were made to align the model's moment arms with those reported in a cadaveric study from Ackland et al. [20]. In the second step, the TSM is validated by comparing its muscle activation predictions against experimental EMG data. The EMG data from the University of Waterloo dataset is useful for validating the TSM, as it allows for a direct comparison between the muscle activation levels of the model and the experimental data. Finally, in the third step, the force contribution of the muscles were analyzed by applying external forces in various directions on the hand of the TSM. These results provide valuable insights on the contributions of individual muscles of the TSM and thereby help with understanding the performance of the TSM.

2
Methods

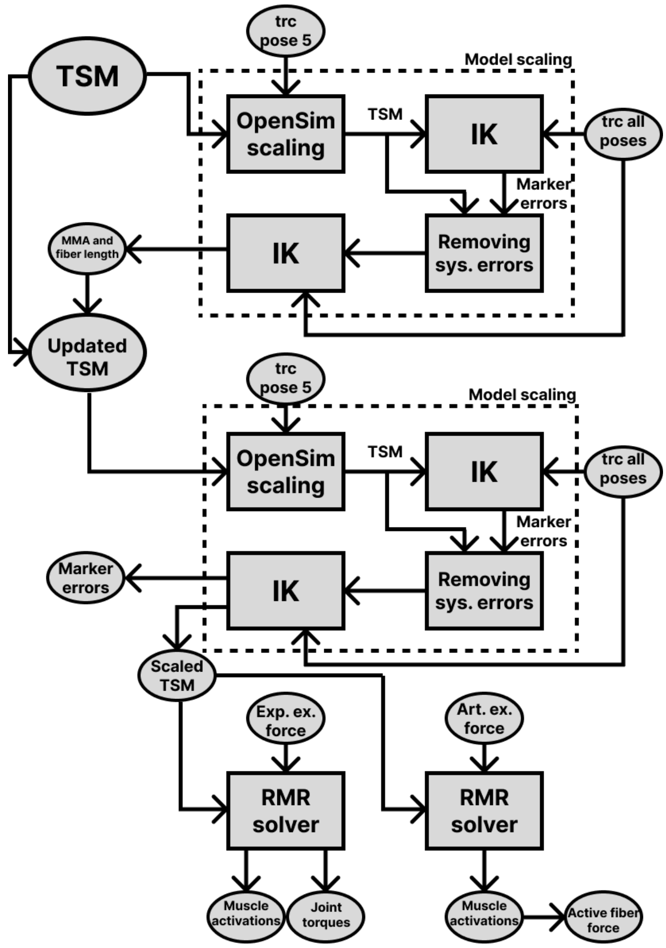

Figure 2.1: Flowchart of the methodology. The top half is used to improve the modeling of the latissimus dorsi and the bottom half is used to investigate the performance of the TSM.

Figure 2.1 shows the methodology that is used in this research. First, the TSM is scaled in four steps: OpenSim GUI scaling, performing inverse kinematics (IK), removing the systematic errors and again performing inverse kinematics. These steps are explained in section 2.3. This scaled model is used to acquire parameters of the latissimus dorsi. With those parameters, the latissimus dorsi is modified, as explained in section 2.4. The updated model is again scaled in four steps and the marker errors are calculated. After this, the muscle activations and joint torque residuals are calculated with an RMR solver (section 2.5). The RMR solver is run with experimental forces in order to verfiy and validate the model. The scaling errors from the scaling process and the joint torque residuals from the RMR solver are used for the verification of the TSM. The moment arm values and the muscle activation levels are used for the validation of the TSM. Lastly, the RMR solver is run with artificial external force. The resulting muscle activations from these experiments have been used to investigate the contributions of individual muscles of the TSM (section 2.6).

2.1. Musculoskeletal Shoulder Model

For this research, a Thoracoscapular Shoulder Model (TSM) is used [15]. The model consists out of 7 bodies and 16 muscles, modeled with 35 muscle segments. The muscle paths are based on Klein Breteler [18] and combined with bundles from Van der Helm [19]. The muscle paths are adjusted to include wrapping surfaces of Ackland et al. [20].

2.2. Experimental dataset

The experimental data used for this research is acquired from a study at the University of Waterloo [23]. In this study, experiments were performed were a subject had to grab a manipulandum and exerts a specific amount of force. The subjects had to reach the required force level in the 2 first seconds of the trial and hold it for the next 5 seconds. The subject had visual feedback of their force direction and magnitude for achieving this task. Twenty male subjects participated in this study and had to perform a total of 120 trials. The trials are divided by 6 pushing directions (to the right, to the left, downwards, upwards, forwards and backwards), 5 poses (low left, high left, low right, high right and center, figure 2.2 and 4 force magnitudes (20N, 30N, 50N and 60N).

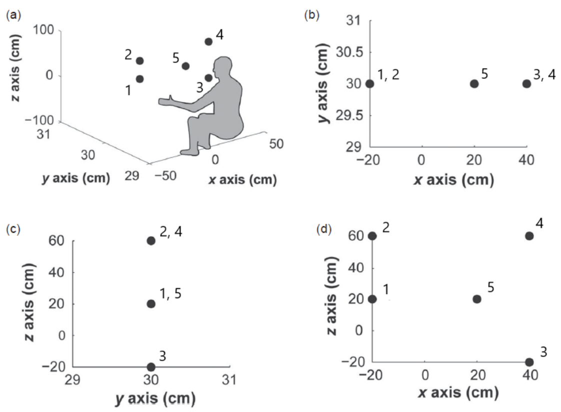

(a) Manipulandum positions [23].

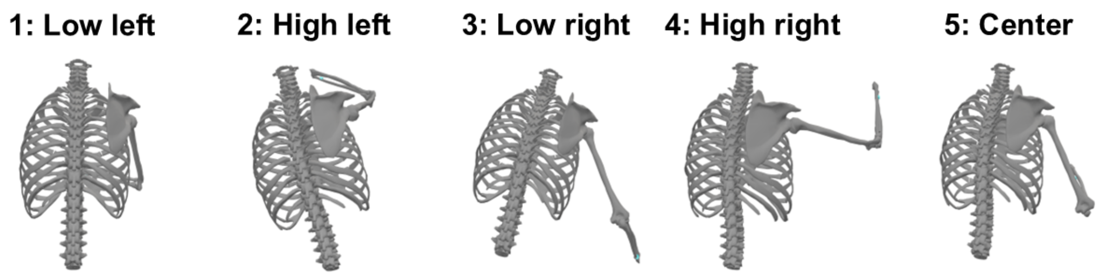

(b) Model poses of TSM in OpenSim.

Figure 2.2: Overview of the 5 different manipulandum positions from the experimental data (a) and the corresponding TSM poses (b). The origin of the coordinate system is positioned at the center of the torso. Position 1 corresponds to the low left pose, position 2 to the high left pose, position 3 to the low right pose, position 4 to the high right pose and position 5 to the center pose.

During each trial, muscle activations, hand forces and motion data was recorded. The muscle activations were measured of the following muscles: anterior, middle and posterior deltoid, biceps brachii, triceps brachii, infraspintus, supraspinatus, clavicular and sternal pectoralis major, latissimus dorsi, serratus anterior and superior, medial an inferior trapezius. They were recorded by EMG sensors with a sample rate of 1500Hz. The hand force were recorded with the manipulandum. Both the magnitude and direction of the force exerted by the hand were collected at 1500Hz. The motion data is recorded with 19 markers placed on the body, with a sampling frequency of 50Hz.

Three sets of Maximal Voluntary Contraction (MVC) measurements were performed per muscle to acquire the maximum voltage levels. For each trial, the raw EMG signals are first filtered, using a 4th order bandpass butterworth filter, with cut-off frequency of 20Hz and 400Hz. Then they are rectified and normalized to the Maximum value of the MVC measurements. For some trials, the maximum activation level after normalization is higher than 1. This trial is then used for calculating the MVC value.

2.3. Model scaling

The model is scaled in four steps, as can be seen in figure 2.1. For each subject, these steps are performed once. The first step uses the Scaling Tool from OpenSim GUI in order to get a rough estimate of the body dimensions. This tool uses the OpenSim base model (section 2.1) and scales the model to the center pose of the Dickerson experiments. The marker pairs used for each respective body can be found in table 2.1. After the first scaling step, inverse kinematics are performed for five trials per subject, one for each position. From this inverse kinematics, the marker errors can be calculated for each position.

Table 2.1: Marker pairs used to calculate the scaling factors.

Body	Direction	Marker pair		Marker pair	
Thorax	X	SS	C7		
	Y	C7	L5		
	Z	SS	ACR		
Clavicle	XYZ	SS	ACR		
Scapula	XYX	ACR	C7		
Humerus	XYZ	ACR	ME	ACR	LE
Ulna	XYZ	US	ME	RS	LE
Radius	XYZ	US	ME	RS	LE

In the third part of the scaling the markers are moved in the scaled model to reduce the marker error. The marker error vectors that follow from the scaling optimizer (step 2) are averaged over the five positions. This mean error is added to the position of the respective marker, moving the marker in the model. This improves the accuracy of the marker, necessary for proper inverse kinematics results, but does not have an impact on the precision of the markers. Inverse kinematics is therefore performed again, with the same trace file that is used during the scaling optimizer, to calculate the marker errors again. As the mean error of the markers is removed, this should be zero now. The mean squared error can therefore be used to see if the marker errors are reduced. In order to speed up calculation time, the data from Dickerson is only used for the time interval of $5.0s < t < 6.5s$. This time interval has the lowest variance in the dataset, as the subject has had time to accustom to the task.

The muscle moment arms from the scaled TSM are calculated in OpenSim. In order to check the accurateness of the moment arms, they are compared to the dataset from Ackland [20]. This dataset contains the minimum and maximum moment arm values for $0°$, $45°$ and $90°$ planar elevation. For all 5 poses, it is checked whether the moment arm values of the TSM lie within the range from the Ackland dataset.

2.4. Improvements latissimus dorsi

The superior, middle and inferior latissimus dorsi muscles of the TSM have been modified. First, the insertion point is moved distally over the humerus, in order to get the insertion points of the three muscle parts closer together. The superior and middle latissimus dorsi have presiously been modeled with 5 path points, the inferior with 4 path points. The intermediate path points are removed and a new ellipsoid is added to the model. This ellipsoid mimics the surface of the thorax and acts as a wrapping surface for the three latissimus dorsi parts. The dimensions and position of this ellipsoid are tweaked to let the latissimus dorsi parts wrap over the thorax as realistic as possible.

Three moving path points, one per muscle part, were added to the model, in order to mimic the narrow part of the latissimus dorsi, close to its insertion point. These insertion points are attached to the thorax and move anteriorly and laterally with increasing planar elevation of the humerus. For this movement is a linear SimmSpline function used. In this function, the position is determined for $0°$ and $180°$ planar elevation and inter- and extrapolated for other planar elevation values. The muscle moment arms of the latissimus dorsi around the glenohumeral joint are compared to a dataset from a cadaveric study performed at the University of Waterloo [20].

According to the force-length relationship, a muscle produces the highest force for a normalized fiber length between 0.80 and 1.30. The tendon slack length of each latissimus dorsi part is altered in order to get the normalized fiber length in this range for all 5 poses.

2.5. RMR solver

A Rapid Muscle Redundancy (RMR) solver, developed by Belli et al. [22] is used to calculate the muscle activations of the shoulder model. For every subject, inverse kinematics is performed for the five different positions (figure 2.2). For each trial, six external force file of the force exerted on the hand are created from the force sensor in the manipulandum. This results in 30 trials per subject: five different poses with each six external force files. With the resulting motion and external force files as input, the RMR solver calculates the joint residuals and the muscle activations by minimizing the cost function 2.1. Here, a_i represents the muscle activation of the muscle i, c_j represents the joint torque actuator of joint j and w_i and w_j represent their respective weights. In total, the RMR solver is run 210 times (seven subjects, five arm poses and six force direction).

$$c = \sum(w_i * a_i^2) + \sum(w_j * T_j^2) \tag{2.1}$$

Table 2.2: Overview of which muscle parts of the TSM model are compared to which muscles of the experimental EMG data.

Musclepart of model	Muscle of experimental data
Anterior deltoid	Anterior deltoid
Middle deltoid	Middle deltoid
Posterior deltoid	Posterior deltoid
Biceps caput longum Biceps caput brevis	Biceps brachii
Triceps caput longum Triceps caput medialis Triceps caput lateralis	Triceps brachii
Inferior infraspinatus Superior infraspinatus	Infraspinatus
Anterior supraspinatus Posterior supraspinatus	Supraspinatus
Clavicular pectoralis major	Superior pectoralis major
Sternal pectoralis major	Middle pectoralis major
Middle latissimus dorsi Inferior latissimus dorsi	Latissimus dorsi
Middle serratus anterior Inferior serratus anterior	Serratus anterior
Superior trapezius	Superior trapezius
Middle trapezius	Middle trapezius
Inferior trapezius	Inferior trapezius

In order to verify the results from the RMR solver, the joint torques of the residual actuators are investigated. The muscle activations from the RMR solver are averaged over the 1.5 seconds trials and compared to the average EMG values of the same time interval (5.0s - 6.5s), by calculating the MAE between the model's muscle activation estimations and the experimental EMG data. Table 2.2 shows which muscles are compared. For some muscle parts of the model, the activation of multiple parts are averaged in order to compare them to the experimental data. For the trend comparison, the increase in muscle activation between the center pose and each outer pose is calculated.

2.6. Muscle analysis

Artificial eternal forces have been created in order to get insight on what muscles are activated in what push and pull directions. Twenty-two external forces with a magnitude of 60N have been created (figure 2.3. Twelve external forces are oriented in the coronal plane and twelve in the transverse plane. The forces are evenly spread with a 30° interval.

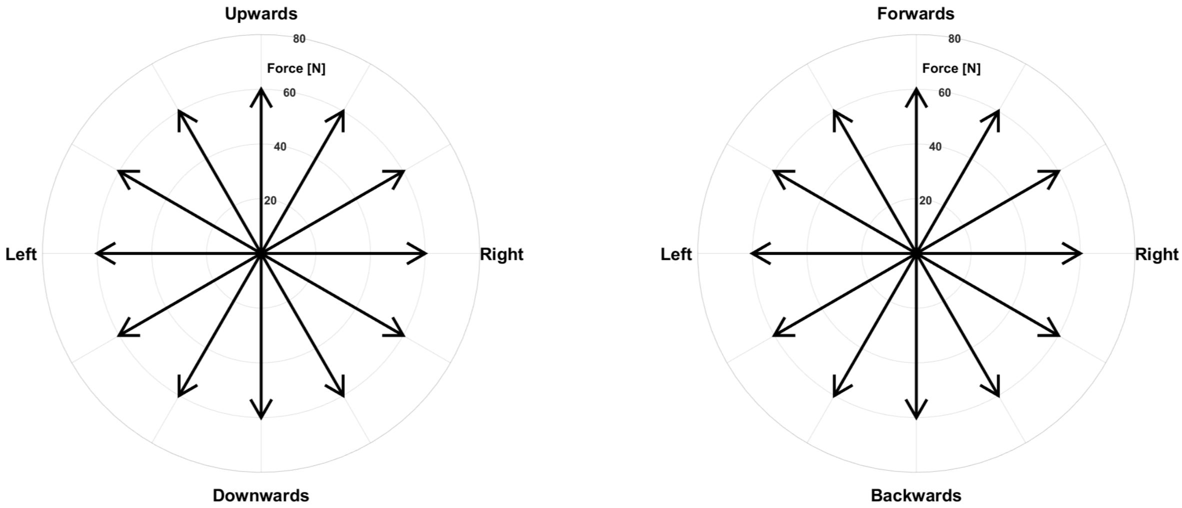

(a) Coronal plane. **(b)** Transverse plane.

Figure 2.3: Directions and magnitude of the artificial external force that is applied on the hand. Each vector shows the external force of 1 trial, with a total of 22 external forces for 22 trials. The external forces directly to the left and to the right are shown in both the coronal plane and transverse plane.

The RMR solver is used again on the TSM, this time with the artificial external forces. For each subject, inverse kinematics is performed in the five positions. The RMR solver is applied 22 times, once for each artificial external force on the TSM once for each of the five poses. With the resulting muscle activation levels, the active fiber force is calculated for all muscles.

3

Results

3.1. Modeling of latissimus dorsi

The superior, middle and inferior latissimus dorsi paths are changed in order to match the muscle moment arms with the data from Ackland et al. [20]. The insertion point of the superior latissimus dorsi is moved distally on the humerus, closer to the middle and inferior latissimus dorsi. The intermediate pathpoints are removed and a new ellipsoid is added to the model, that is used as a wrapping surface for all three muscle parts. A moving path point is added close to the insertion point, in order to merge the three muscle parts close together. The moving path points are attached to the thorax and moves anteriorly and laterally with an increasing planar elevation of the humerus, using a simmspline function. The exact locations and functions can be found in appendix A. The tendon slack length is set to 0.01m for all three latissimus dorsi muscles, in order to increase their normalized fiber lengths.

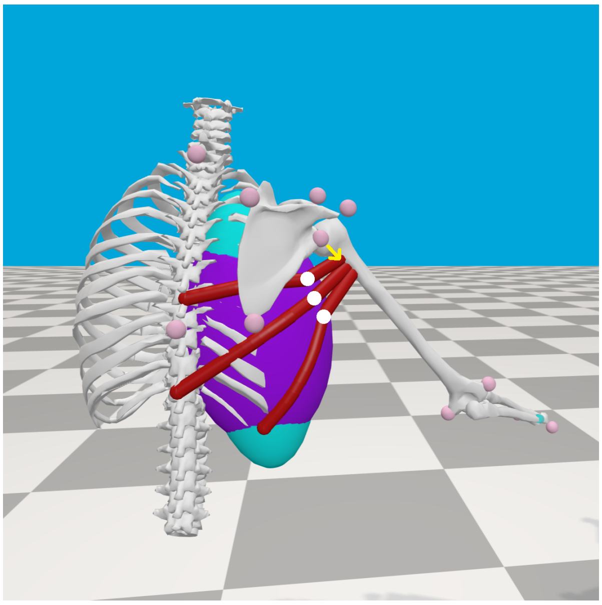

Figure 3.1: Changes to the path of the superior, middle and inferior latissimus dorsi muscle. The yellow arrow points from the old insertion point of the superior latissimus dorsi to its new insertion point, the purple ellipsoid is used for wrapping the latissimus dorsi and the white circles are the new moving path points.

3.2. Verification

3.2.1. Scaling errors

Subject KWG did not have available data for markers SS and XP in the low right pose. The mean error is therefore calculated with the position data of the other four poses for these two markers for subject KWG.

After the OpenSim GUI scalig, the averaged marker error range from 11mm to 60mm. After removing the mean error of each marker, the error is reduced for all subjects, as can be seen in table 3.1. For seven subjects the error is below 12mm. The error for subject DRM is with an average of 16.4 significantly higher than the error for the other subjects. This subject will not be used for further analysis of the results.

Position	ACC	AWW	BRD	CRT	DRM	KJM	KWG	MBD
low left	9.0 ± 7.5	9.3 ± 8.3	8.5 ± 9.2	10.1 ± 9.2	20.0 ± 13.3	8.3 ± 5.6	10.6 ± 5.7	9.0 ± 7.8
high left	12.4 ± 7.3	12.8 ± 8.6	7.5 ± 5.5	12.6 ± 9.3	13.1 ± 10.5	9.4 ± 4.3	10.7 ± 7.0	12.5 ± 8.0
low right	15.4 ± 6.7	15.5 ± 6.4	8.3 ± 5.5	19.1 ± 8.0	14.9 ± 8.3	12.8 ± 6.5	14.8 ± 11.8	16.0 ± 6.3
high right	8.0 ± 4.6	11.1 ± 4.8	10.7 ± 8.6	11.9 ± 4.7	16.3 ± 11.4	8.7 ± 4.7	9.5 ± 4.3	10.8 ± 6.2
center	6.2 ± 2.7	8.8 ± 2.9	5.7 ± 3.0	5.8 ± 3.5	17.6 ± 12.6	9.2 ± 3.8	8.4 ± 3.4	9.1 ± 3.8
Average	10.2 ± 6.8	11.5 ± 6.9	8.1 ± 6.8	11.9 ± 8.3	16.4 ± 11.3	9.7 ± 5.2	10.7 ± 7.1	11.5 ± 6.9

Table 3.1: Average error of all markers of inverse kinematics after removing the systematic error of the markers in mm.

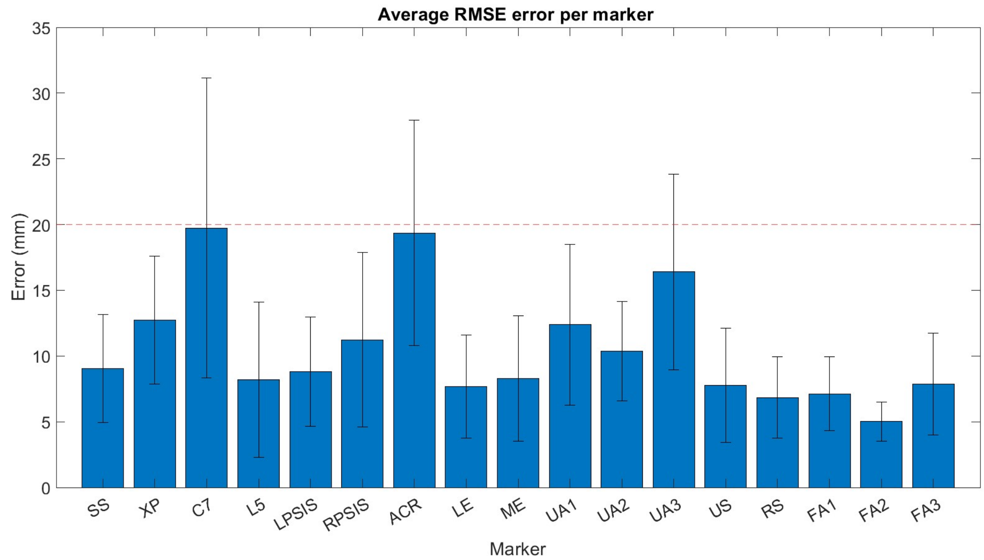

Figure 3.2: Averaged marker error for each individual marker. The error is averaged over the five trials and seven subjects. The errorbars show the standard deviation.

Figure 3.2 shows the average error per marker. The average error of markers C7, ACR and UA3 is significantly higher than for the other markers

3.2.2. Normalized fiber length

Table 3.2 shows the normalized fiber length of the latissimus dorsi muscle for the original and updated model. For the superior and inferior latissimus dorsi, the normalized fiber length increases from an average of 0.72 and 0.69 to an average of 0.99 and 1.00 respectively. The normalized fiber length of the inferior latissimus dorsi also increases, but only to an average of 0.74.

Table 3.2: Normalized fiber length of the latissimus dorsi of the original and updated model, averaged over all trials.

Pose	Original model			Updated model		
	LatsS	LatsM	LatsI	LatsS	LatsM	LatsI
Low left	0.72	0.70	0.55	0.99	1.00	0.73
High left	0.76	0.79	0.67	1.07	1.10	0.83
Low right	0.69	0.63	0.49	0.96	0.94	0.69
High right	0.73	0.73	0.63	1.01	1.04	0.79
Center	0.68	0.62	0.42	0.95	0.94	0.69

3.2.3. Residual torques

Table 3.3 shows the joint torque residuals for the joint actuators for the RMR solver with external forces from measurements. For clavicle protraction, the torques are significantly higher than for the other actuators. The torques are higher in the high left pose than in the other poses. The torques produced by the muscles are still higher than the torques produced by the actuators (section 3.4), except for the pronation-supination actuator in the high left pose. As there are no muscles in the forearm, this actuator is needed to stabilize the forearm.

Table 3.3: Residual torques of the joint actuators during the RMR solver in Nm. For every pose, the torques are averaged over 42 trials (6 external force directions, for 7 subjects).

Actuator	Low left	High left	Low right	High right	Center
clavicle protraction	0.23 ± 0.17	0.26 ± 0.21	0.10 ± 0.12	0.16 ± 0.11	0.74 ± 0.24
clavicle elevation	0.08 ± 0.06	0.13 ± 0.08	0.07 ± 0.02	0.04 ± 0.02	0.01 ± 0.02
scapula abduction	0.00 ± 0.00	0.01 ± 0.02	0.00 ± 0.00	0.00 ± 0.00	0.00 ± 0.00
scapula elevation	0.00 ± 0.00	0.01 ± 0.01	0.00 ± 0.00	0.00 ± 0.00	0.00 ± 0.00
scapula upward rotation	0.00 ± 0.01	0.02 ± 0.03	0.00 ± 0.00	0.00 ± 0.00	0.00 ± 0.00
scapula winging	0.00 ± 0.01	0.02 ± 0.02	0.00 ± 0.00	0.00 ± 0.00	0.00 ± 0.00
planar elevation	0.00 ± 0.01	0.01 ± 0.02	0.00 ± 0.00	0.00 ± 0.00	0.00 ± 0.00
shoulder elevation	0.00 ± 0.00	0.01 ± 0.02	0.00 ± 0.00	0.00 ± 0.00	0.00 ± 0.00
axial rotation	0.03 ± 0.05	0.07 ± 0.06	0.00 ± 0.00	0.00 ± 0.00	0.00 ± 0.01
elbow flexion	0.01 ± 0.02	0.14 ± 0.10	0.00 ± 0.00	0.00 ± 0.01	0.00 ± 0.02
pronation-supination	0.07 ± 0.13	0.70 ± 0.53	0.00 ± 0.00	0.01 ± 0.06	0.00 ± 0.01

3.3. Validation

3.3.1. Moment arms

Figure 3.3 shows the muscle moment arms of the superior, middle and inferior latissimus dorsi from the cadaveric study from Ackland et al. [20] and from the simulation results. In the right and middle poses, the moment arms from simulation results show a similar trend as the moment arms from the cadaveric study. The moment arms of the middle latissimus dorsi are smaller in magnitude, but they are higher when the arm is raised (higher abduction angles), similar to the cadaveric study. In the left poses, the moment arms form the simulation results are significantly higher than for the cadaveric study. Only the superior latissimus dorsi matches for the low left pose.

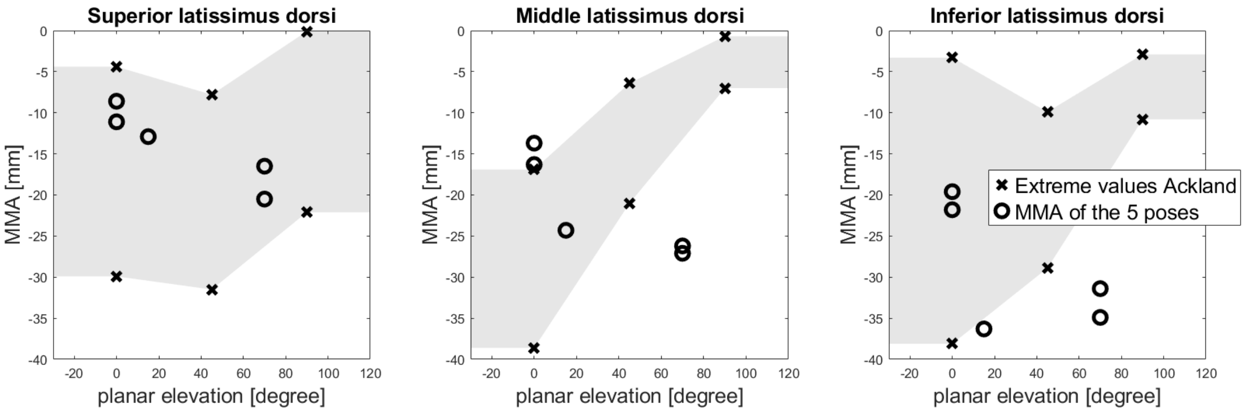

Figure 3.3: Muscle moment arms with respect to shoulder elevation of the latissimus dorsi. The circles are the moment arms of the TSM, the crosses are the minimum and maximum value from a cadaveric study [20]. The shaded area marks the range where the moment arm values should stay within, according to the cadaveric study.

3.3.2. Muscle activations

The MAE between the muscle activations from the RMR solver and EMG measurements are calculated for the old and updated model. The MAE are averaged per pose (table 3.4). The center and low right pose have an average MAE lower than 0.10 for respectively 12 and 11 out of 13 muscles, while the high left pose only has an MAE lower than 0.10 for the Sternal pectoralis major. There is no significant improvement of MAE after the improvements of the latissimus dorsi.

The triceps, infraspinatus, sternal pectoralis major and superior trapezius have the lowest MAE on average. The deltoid, biceps, supraspinatus, clavicular pectoralis major and serratus anterior have a low MAE for the low right and center pose, but their MAE is significantly higher for either the high left, or high right pose. This results in a higher average MAE for these muscles. The latissimus dorsi and inferior and middle trapezius have a low MAE for all 5 poses.

	Low left	High left	Low right	High right	Center	Average
Anterior deltoid	0.10 ± 0.10	0.21 ± 0.13	0.06 ± 0.05	0.13 ± 0.10	0.04 ± 0.03	0.11 ± 0.11
Middle deltoid	0.12 ± 0.13	0.21 ± 0.11	0.07 ± 0.05	0.11 ± 0.08	0.03 ± 0.03	0.11 ± 0.11
Posterior deltoid	0.14 ± 0.16	0.33 ± 0.30	0.07 ± 0.10	0.08 ± 0.08	0.05 ± 0.08	0.14 ± 0.20
Biceps	0.13 ± 0.15*	0.21 ± 0.14	0.07 ± 0.06	0.08 ± 0.06*	0.05 ± 0.06	0.11 ± 0.11*
Triceps	0.09 ± 0.08	0.11 ± 0.09	0.09 ± 0.07	0.09 ± 0.10	0.07 ± 0.09	0.09 ± 0.09
Infraspinatus	0.07 ± 0.09	0.13 ± 0.09	0.09 ± 0.12	0.12 ± 0.07	0.07 ± 0.08	0.09 ± 0.10
Supraspinatus	0.05 ± 0.12*	0.18 ± 0.11	0.07 ± 0.07	0.12 ± 0.10*	0.09 ± 0.10	0.10 ± 0.10*
Clavicular pectoralis major	0.15 ± 0.11	0.23 ± 0.15	0.05 ± 0.05	0.09 ± 0.10	0.05 ± 0.05	0.11 ± 0.11
Sternal pectoralis major	0.10 ± 0.08	0.09 ± 0.08	0.07 ± 0.07	0.04 ± 0.03	0.05 ± 0.04	0.07 ± 0.07
Latissimus dorsi	0.18 ± 0.12	0.13 ± 0.09	0.16 ± 0.10	0.12 ± 0.10	0.09 ± 0.07	0.13 ± 0.12
Serratus anterior	0.17 ± 0.09	0.25 ± 0.16	0.07 ± 0.08	0.22 ± 0.13	0.06 ± 0.07	0.15 ± 0.14
Inferior trapezius	0.10 ± 0.08	0.18 ± 0.11	0.13 ± 0.11	0.25 ± 0.13	0.13 ± 0.11	0.16 ± 0.12
Middle trapezius	0.10 ± 0.12	0.12 ± 0.10	0.16 ± 0.14	0.21 ± 0.13	0.15 ± 0.13	0.15 ± 0.13
Superior trapezius	0.05 ± 0.03	0.17 ± 0.13	0.03 ± 0.04	0.09 ± 0.08	0.04 ± 0.04	0.08 ± 0.09

Table 3.4: MAE of the muscle activation levels of the updated model. The average and standard deviation of the MAE in each pose are calculated over 7 subjects and 6 directions. If the MAE decreased with more than 0.02, the MAE is marked with an asterisk (*).

3.4. Active fiber forces

The muscle activations of the TSM with artificial external forces have been calculated by the RMR solver. The TSM pushes in 24 directions, 12 in the coronal plane and 12 in the transverse plane. For each muscle, the active fiber force is calculated. For every pose, the 10 muscles that produce the highest active fiber force in are shown in figure 3.4. Except for the center pose, the middle deltoid produces the highest force, with a force 1.5 to 2.5 times larger than the second-biggest force. As the low right and center pose have the best validation results, the active fiber forces of those two poses are further investigated. Table 3.5 lists which muscles achieve the highest force in the six push and pull directions in figure 3.4c and figure 3.4e.

Table 3.5: List of muscles with the highest active fiber force for each push and pull directions. For each direction, the muscles that achieve the highest active fiber force in the center pose and low right pose in each direction are listed. The muscles are ordered alphabetically.

Left	Right	Downwards	Upwards	Forwards	Backwards
Biceps brevis Corachobrachialis Middle pectoralis major Inferior subscapularis Middle subscapularis Triceps longus	Middle deltoid Inferior infraspinatus Superior infraspinatus Triceps longus Superior trapezius scapularis	Middle deltoid Teres major Triceps longus Superior infraspinatus Triceps longus Superior trapezius scapularis	Anterior deltoid Middle deltoid Inferior infraspinatus	Anterior deltoid Middle deltoid Middle serratus anterior	Middle deltoid Teres major Triceps longus

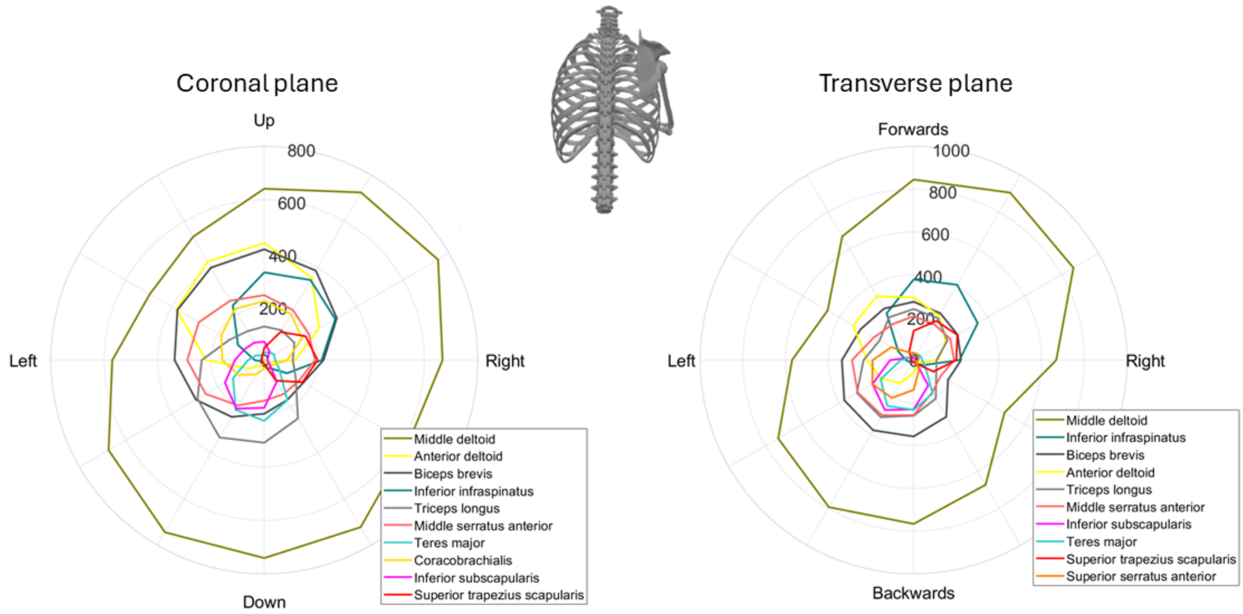

(a) Low left pose.

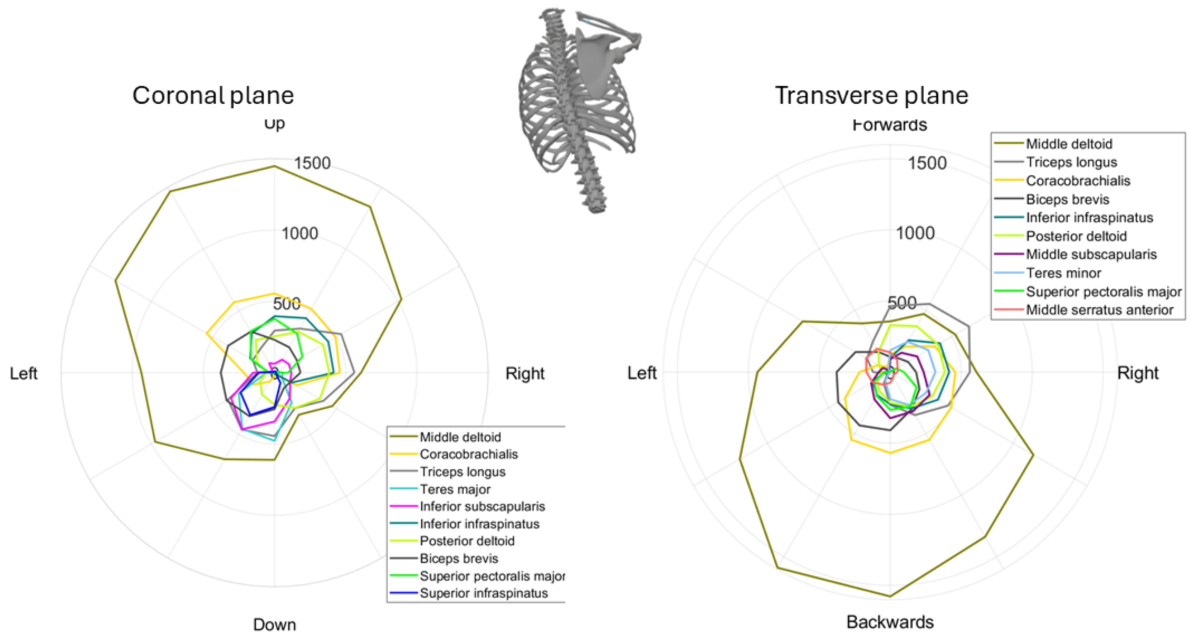

(b) High left pose.

Figure 3.4: Polar plots with the active muscle force when pulling in the coronal and transverse plane. The different directions indicate the direction the model is pushing towards. The 10 muscles with the highest active force are shown. Note that the scale varies for each graph.

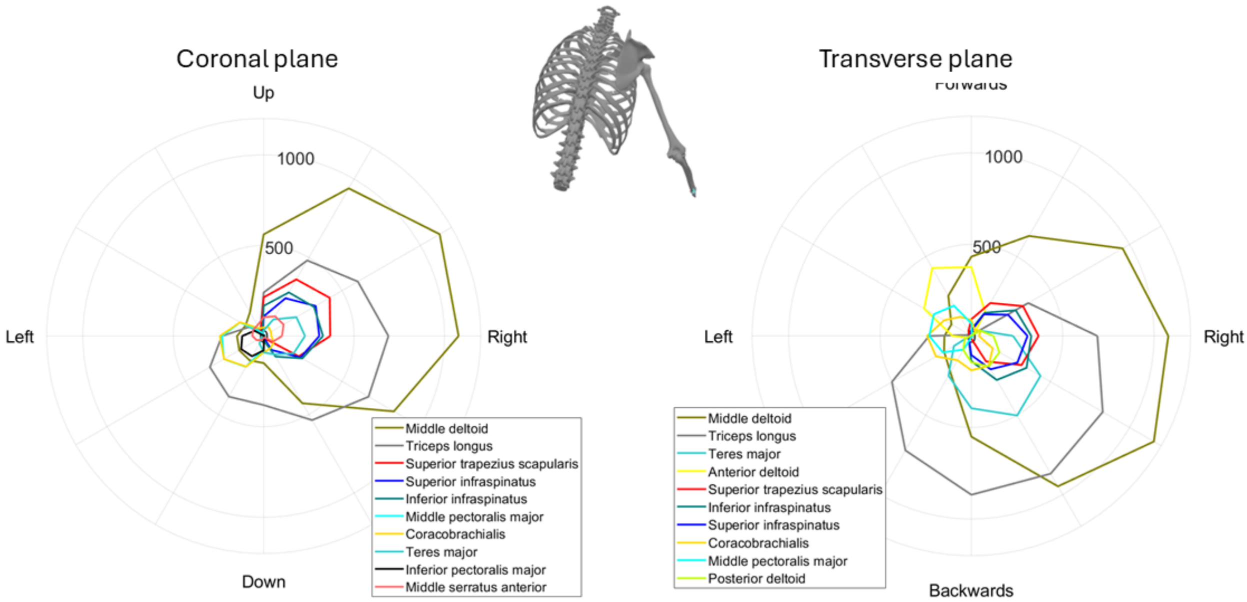

(c) Low right pose.

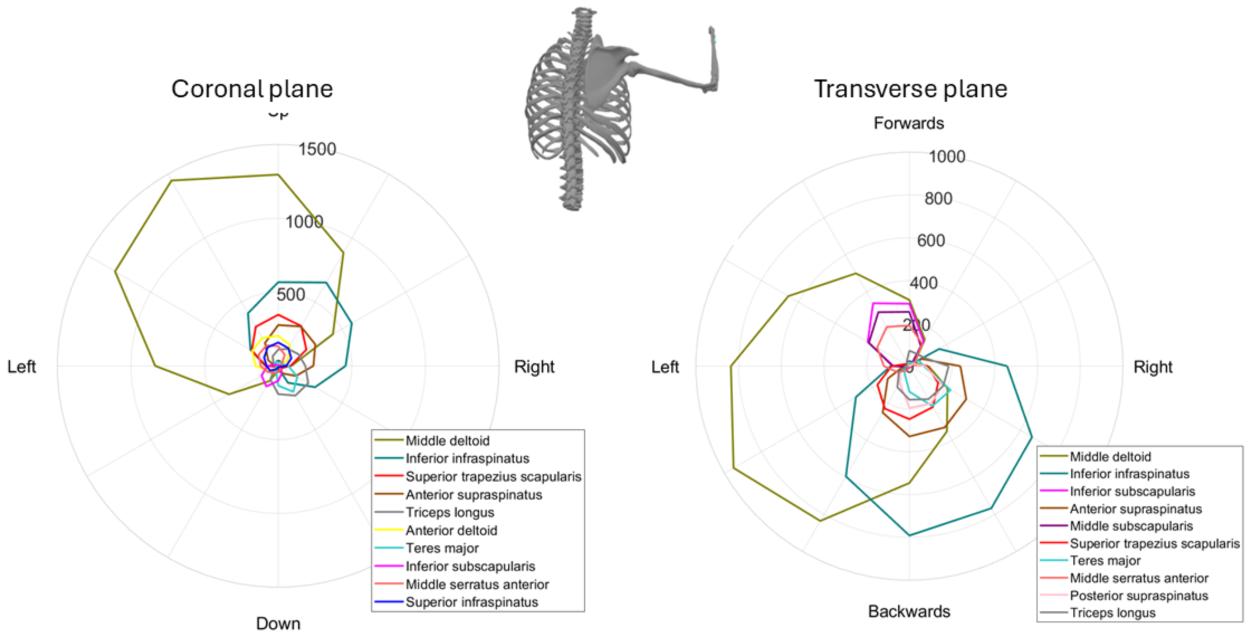

(d) High right pose.

Figure 3.4: (continued).

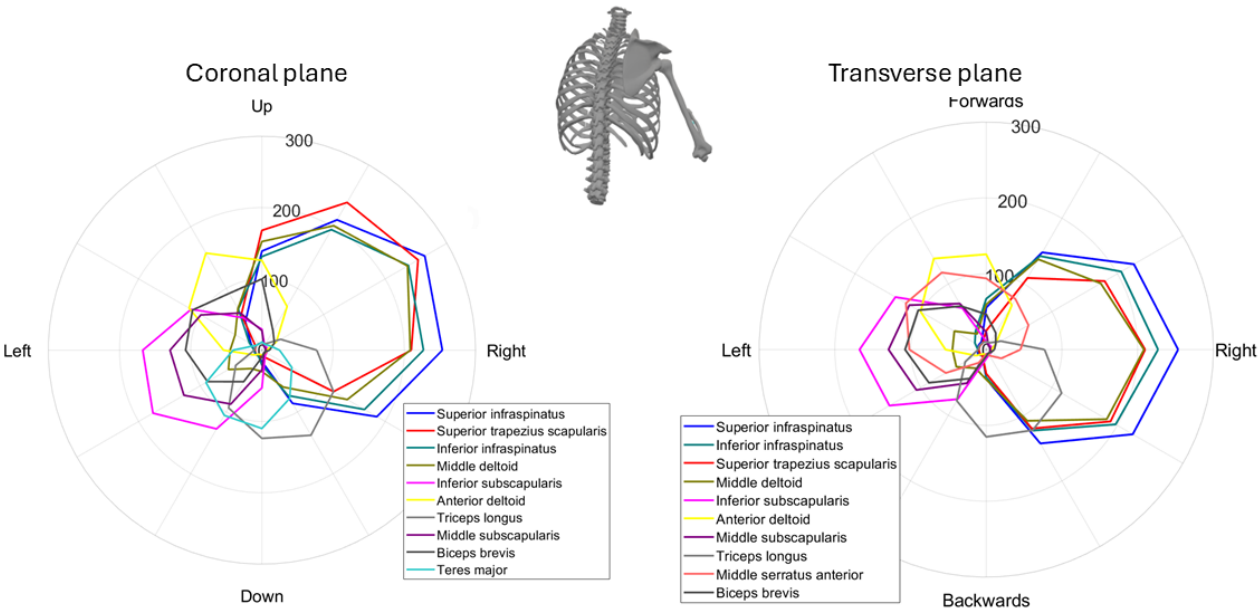

(e) Center pose.

Figure 3.4: (continued).

4

Discussion

4.1. Experimental data

The experimental data from the University of Waterloo [23] provided a dataset of 20 subjects, with 120 trials for each subject, of which 30 trials of 8 subjects were used. The dataset consists of motion data, external force measurements on the manipulandum and EMG data. The external force data that has been collected during this research has a lot of variance. The participants of the experiments received the task to maintain a force of 60N in a specified direction. This resulted in large variations of the direction of the external force. These experimental forces were suitable to verify and validate the TSM, but are less reliable to use to determine which muscles produce the highest force in varying pulling directions. As a result, artificial external forces have been created to investigate the muscle force contributions (figure 3.4).

The EMG measurements have been used to compare the muscle activation levels of the RMR solver to. EMG values of maximum voluntary contraction measurements have been used to normalize the EMG measurements, but the muscle activation levels of the muscles obtain values above 1 after normalization. Therefore, the maximum EMG value that is measured is taken as MVC value. This makes the EMG measurements less reliable to use for the comparison of the activation levels of the RMR solver.

In addition, several considerations were made when selecting which muscles to compare against the EMG data. For the biceps, triceps, infraspinatus and supraspinatus, the EMG values are compared to the average muscle activation levels of all muscle parts. These muscles are rather small and the exact placement of the EMG sensor was not clear. The sternal pectoralis major, latissimus dorsi and serratus anterior are relatively big muscles. One EMG sensor will not be able to measure activity from all three muscle parts. Therefore, the middle and inferior parts of these muscles are used to compare to the EMG values, as these parts are closest to the position of the EMG sensors.

4.2. Model scaling

For most markers, the average RMSE is smaller than 20mm (figure 3.2), which can be assumed to be good [9]. The markers C7, ACR and UA3 have RMSE's larger than 20mm. The ACR marker is especially important for the model, as it is placed on the acromion. It is impossible to determine all three 3 degrees of freedom of the scapula with one marker on the shoulder. This makes the motion data from the study at Universit of Waterloo [23] less suitable to use with the DSEM model. One way to improve the motion data is to use an acromion marker cluster, consisting of three markers instead of one [24].

The marker RMSE after GUI scaling is two times larger for subject DRM than for the other subjects.

The scaling factor of $thorax_y$ is 1.21, while the scaling factor of $thorax_z$ is 0.75. This indicates a wide, slim body type for subject DRM, as can be seen in figure 4.1. The scapula cannot be placed correctly on the thorax for this body type. There is however no data available on the length and body type of each individual, so there could also be another underlying cause.

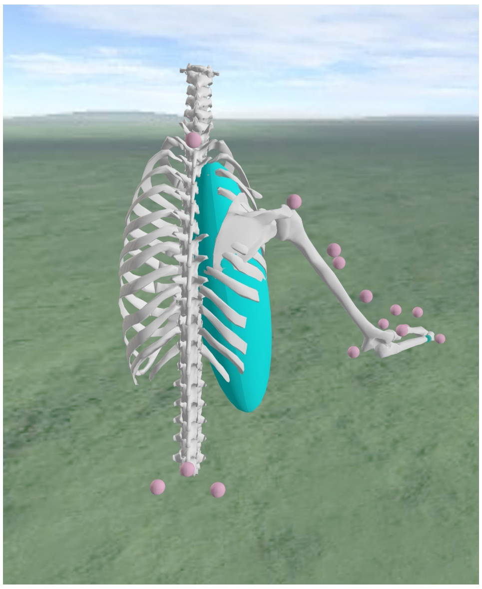

Figure 4.1: OpenSim model of subject DRM after GUI scaling.

The marker RMSE is smallest in the center pose, which is also the pose that is used for the scaling factors in the scaling process. Even though the errors for all positions are combined when removing the systematic error, the RMSE is on average still smallest in the center pose (table 3.1). During the scaling process, the model therefore overfits to the center pose. Instead of using only one trial of the center pose to obtain the scaling factors, the scaling results can be improved by using trials of every pose to obtain the scaling factors.

4.3. Modeling of latissmus dorsi

After the changes, the three latissimus dorsi muscles are modeled with 3 pathpoints instead of 4 or 5, These path points were placed a few centimeters around the thorax. Because of this, the ellipsoid that previously has been used to wrap the latissimus dorsi around the thorax did not interfere with the path of the latissimus dorsi. By removing the intermediate path points and adding a new ellipsoid, that is wider than the previous ellipsoid, the latissimus dorsi curves more smoothly around the thorax.

The added moving path points do not fully replicate real-life movement patterns. The moving path points only moves with planar elevation of the humerus, but in order to mimic real-life movement of the latissimus dorsi better, this path point should also move superiorly with humeral elevation.

The tendon slack length is set to 1 cm, as the tendon won't produce much force anymore when making it shorter. Even though the normalized fiber improved for all three muscles, the tendon slack length is not based on real latissimus dorsi muscles.

4.4. Residual torques

The joint torque residuals are the highest in the high left pose (table 3.3). When reaching for the manipulandum, the subjects move their whole upper body to the left, as can be seen in figure 4.2. The residual torques are higher when pushing to the right. For this trial, the subjects move their body less to the left. One reason for this can be that the model has trouble with capturing the leaning movement of the upper body during inverse kinematics for these trials, resulting in a less accurate motion file.

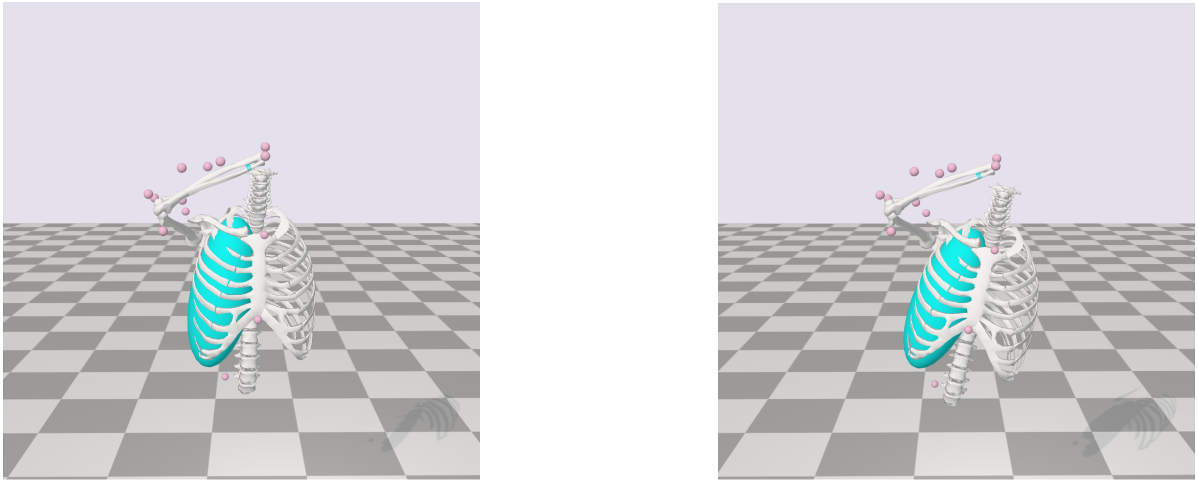

(a) Pulling to the right **(b)** Pushing to the left

Figure 4.2: Body positions of subject ACC with its arm in the high left pose. (a) shows the motion data for the trial where the subject is pulling to the right. For (b), the subject is pushing to the left. When pushing to the left, the subject is leaning to the left.

4.5. Moment arms

According to the moment arms from the dataset from Ackland et al. [20], the middle latissimus dorsi has a larger moment arm than the inferior latissimus dorsi. However, the inferior latissimus dorsi is placed distal to the middle latissimus dorsi, further away from the glenohumeral joint. Therefore, the moment arm of the inferior latissimus dorsi is expected to be larger than the moment arm of the middle latissimus dorsi. This indicates that the insertion point of the inferior latissimus dorsi should have a more oblique orientation.

At lower planar elevation angles, the moment arms of the latissimus dorsi corresponds to the dataset from Ackland et al. [20]. However, for the two left poses, the moment arms are larger than the maximum measured value from the cadaveric study. The moving path point that is added to the TSM moves anteriorly with an increase in planar elevation, in order to move the path point around the thorax. The spline function that is used for this movement is linear, while the thorax has a more ellipsoidal shape. Using a higher-order spline function will ensure that the moving path point of the latissimus dorsi is moved more smoothly around the thorax. This can improve the moment arm of the latissimus dorsi for high planar elevation angles.

Only the angles of the glenohumeral joint are investigated during the comparison of the muscle moment arms, but the position of the scapula and clavicle is ignored. Variations in scapular or clavicular positioning have an impact on the moment arms of the latissimus dorsi. This may explain some of the differences between the moment arms of the latissimus dorsi from the model and from the cadaveric study.

4.6. Mean absolute error

The MAE is a useful metric for comparing the muscle activations to EMG data. After the modeling of the latissimus dorsi in the TSM is improved, the MAE decreases for only the biceps and infraspinatus, but stays the same for the latissimus dorsi. Even though the muscle moment arms and normalized fiber length show an improvement of the latissimus dorsi, the MAE does not improve for the experiments performed in this study. Therefore, it can not be concluded whether the changes of the latissimus dorsi result in an improvement of the TSM.

The MAE values deviate a lot between the different poses. The low right and center poses have low MAE values (table 3.4. The planar elevation and humeral elevation angles for these two poses are below 25° and 45° respectively. Therefore, the reliability of the TSM is good for low planar elevation and humeral elevation angles. For the low left and high left poses, the planar elevation of the humerus is around 90°. For this planar elevation angle, the MAE increases for all muscles except the trapezius. The deltoid, biceps and serratus anterior have the biggest increase of MAE. The high left and high right pose both have a humeral elevation above 70°. For these poses, the serratus anterior, inferior trapezius and supraspinatus have he biggst increase in MAE. The sternal pectoralis major is the only muscle where the MAE decreases for an increase in humeral elevation. Overall, the MAE show poor to mediocre agreement of the muscle activations with the EMG values in the low left, high left and high right poses. Therefore, the validation of the TSM is inconclusive for high shoulder elevation and planar elevation angles. The agreement of MAE is good for the low right and center poses. The accuracy of the TSM is trustworthy when the shoulder elevation and planar elevation angles are low.

4.7. Active fiber forces

The middle deltoid produces significantly higher force than all other muscles in 4 out of 5 analyzed poses. A study from De Groot et al. [25] previously investigated isometric shoulder muscle activations patterns. They applied an external force on the hand in 20 directions in the coronal plane and investigated the muscle activation patterns in this plane. They found that the middle deltoid has the highest activation when pushing upwards and to the right, which is in line with the results from figure 3.4. However, they found little to no activation when pushing downwards and to the left, while in this study the middle deltoid still produces a large force in these directions. This can indicate that the middle deltoid plays a major role in stabilizing the shoulder in the TSM, but the exact role of the middle deltoid is unsure from this experiments. New experiments with dynamic movement can help determining what the role of the middle deltoid is in the TSM.

Table 3.5 reports which muscles have the highest active fiber force for which push and pull direction. As De Groot et al. [25] reported the muscle activation levels in the coronal plane, the four directions in this plane (left, right, up and down) can be validated to this dataset. The infraspinatus, anterior and posterior deltoid and pectoralis major are activated in similar directions in this research as in De Groot et al. . For the trapezius muscle, the TSM shows a high active fiber force in the superior part, while De Groot et al. shows a high activation in the inferior part when pushing upwards. This can partly be explained by the maximum isometric force of these two muscles in the model. The superior trapezius has an isometric force fo 1043N in the TSM, while the isometric force of the inferior trapezius is only 414N. This means that the superior trapezius exerts a bigger active fiber force than the inferior trapezius, for the same activation level. However, the inferior trapezius reaches an activation level of 0.9 with an external force of 20N. The active fiber force of the inferior trapezius in the TSM is therefore lower than can be expected.

In general, the active fiber forces are higher when pushing upwards and to the right than when pulling downwards and to the left. This difference is best visible in figure 3.4e. This phenomenon can partially be explained by the experimental set-up. During the experiments, the arm of the subject has no support. The muscles in the TSM do not only have to counteract the external force, but also the weight of the arm itself. With the total weight of the arm being 3.5kg, this results in an extra force of 35N pulling the arm downwards. For the experiments where the TSM pushes upwards, the external force is also exerted in the downwards direction. The total force applied on the TSM is 95N. For the experiments where the TSM pulls downwards, the force is exerted in the opposite direction. The total force applied is just 25N for these experiments. The TSM has to counteract a force that is almost 4 times higher when pushing upwards than pulling downwards. In the study from De Groot et al. [25], there is a support below the elbow that can counteract the weight of the arm. The difference in muscle activation levels is smaller in those experiments.

As the active fiber forces are not only higher in the upwards direction, but also in the right direction, the elbow support does not explain this phenomenon fully. The muscles that produce the highest active fiber force for the pulling directions are the subscapularis, teres major, and biceps. These muscles have a deep position in the TSM. The infraspinatus, superior trapezius and middle deltoid produce the highest force for the pushing directions. These muscles have a superficial position in the TSM. For pulling, the line of actions of the muscles that are activated are closer together (figure 4.3). Because of this, less total muscle force is required to stabilize the TSM for a pulling motion than for a pushing motion.

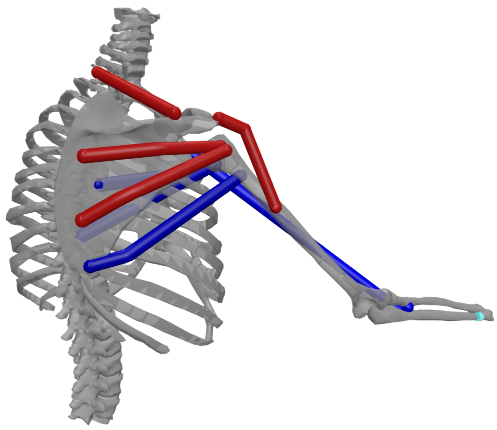

Figure 4.3: Muscles that produce the highest active fiber force for pulling and for pushing. The inferior and middle subscapularis, teres major and biceps produce the highest force for pulling and are colored blue. The inferior and superior infraspinatus, Superior trapezius scapularis and middle deltoid produce the highest force for pushing and are colored red.

5 Conclusion

The aim of this research was to get a better understanding of the performance of the TSM in a wider range of motion. The dataset from the University of Waterloo provided useful measurements to test the model with isometric movements in 5 different poses. The marker errors of the scaling process and the joint torque residuals from the RMR solver have been used for the verification of the TSM. From these results can be concluded that the TSM is correctly implemented and represents the underlying model accurately. After this, the muscle moment arms and muscle activation levels have been compared to experimental data. The muscle path of the latissimus dorsi has been changed, which improved the moment arms of the latissimus dorsi. For high planar elevation angles, this moment arm is still relatively high. The MAE of the muscle activation levels show a high variance for three of the five poses. The two poses where the shoulder has low planar elevation and humeral elevation angles have a low MAE value From this experiments can be concluded that the TSM performs well for low humeral planar elevation and low humeral elevation angles. The performance decreases when the planar elevation or humeral elevation angle increases.

With this research, a better understanding of the performance of the TSM is acquired, but new experiments with dynamic movements are needed in order to be able to determine in which range of motion the TSM performs well. For these experiments, it is important that the orientation of the scapula will be measured. In this study, the movements of the scapulothoracic joint and acromioclavicular joint is not investigated, but they have an influence on the muscle activations of the RMR solver. By tracking the scapula during dynamic movements, the effect of these joints on the performance of the TSM can be investigated.

Bibliography

[1] P. Reilly, I. Macleod, R. Macfarlane, J. Windley, and R. Emery, “Dead men and radiologists don’t lie: A review of cadaveric and radiological studies of rotator cuff tear prevalence,” *The Annals of The Royal College of Surgeons of England*, vol. 88, no. 2, pp. 116–121, 2006, PMID: 16551396. [Online]. Available: `https://doi.org/10.1308/003588406X94968`.

[2] A. Yamamoto, K. Takagishi, T. Osawa, *et al.*, “Prevalence and risk factors of a rotator cuff tear in the general population,” *Journal of Shoulder and Elbow Surgery*, vol. 19, no. 1, pp. 116–120, 2010, ISSN: 1058-2746. [Online]. Available: `https://www.sciencedirect.com/science/article/pii/S1058274609002043`.

[3] T. Teunis, B. Lubberts, B. T. Reilly, and D. Ring, “A systematic review and pooled analysis of the prevalence of rotator cuff disease with increasing age,” *Journal of Shoulder and Elbow Surgery*, vol. 23, no. 12, pp. 1913–1921, 2014, ISSN: 1058-2746. [Online]. Available: `https://www.sciencedirect.com/science/article/pii/S1058274614004480`.

[4] B. W. Jeffrey D. Osborne Ashok L. Gowda and J. M. Wiater, “Rotator cuff rehabilitation: Current theories and practice,” *The Physician and Sportsmedicine*, vol. 44, no. 1, pp. 85–92, 2016, PMID: 26548634. [Online]. Available: `https://doi.org/10.1080/00913847.2016.1108883`.

[5] T. A. Sgroi and M. Cilenti, “Rotator cuff repair: Post-operative rehabilitation concepts,” *Current reviews in musculoskeletal medicine*, vol. 11, pp. 86–91, 2018.

[6] C. Littlewood, M. Bateman, D. Clark, *et al.*, “Rehabilitation following rotator cuff repair: A systematic review,” *Shoulder & elbow*, vol. 7, no. 2, pp. 115–124, 2015.

[7] O. A. van der Meijden, P. Westgard, Z. Chandler, T. R. Gaskill, D. Kokmeyer, and P. J. Millett, “Rehabilitation after arthroscopic rotator cuff repair: Current concepts review and evidence-based guidelines,” *International journal of sports physical therapy*, vol. 7, no. 2, p. 197, 2012.

[8] L. Peternel, A. Seth, J. Prendergast, T. Driessen, and S. Balvert, “Ptbot: Biomechanics-aware physical therapy robot,” 2023.

[9] OpenSim Project, *Opensim documentation: User guide and reference documentation*, Accessed: 2024-11-07. [Online]. Available: `https://simtk-confluence.stanford.edu`.

[10] A. Erdemir, S. McLean, W. Herzog, and A. J. van den Bogert, “Model-based estimation of muscle forces exerted during movements,” *Clinical Biomechanics*, vol. 22, no. 2, pp. 131–154, 2007, ISSN: 0268-0033. [Online]. Available: `https://www.sciencedirect.com/science/article/pii/S0268003306001835`.

[11] B. H. Thacker, “Asme standards committee on verification and validation in computational solid mechanics,” *Report, The American Society of Mechanical Engineers (ASME) Council on Codes and Standards (Sep 2001)*, vol. 8, 2001.

[12] J. L. Hicks, T. K. Uchida, A. Seth, A. Rajagopal, and S. L. Delp, “Is my model good enough? best practices for verification and validation of musculoskeletal models and simulations of movement,” *Journal of biomechanical engineering*, vol. 137, no. 2, p. 020 905, 2015.

[13] M. E. Lund, M. de Zee, M. S. Andersen, and J. Rasmussen, “On validation of multibody musculoskeletal models,” *Proceedings of the Institution of Mechanical Engineers, Part H: Journal of Engineering in Medicine*, vol. 226, no. 2, pp. 82–94, 2012, PMID: 22468460. [Online]. Available: `https://doi.org/10.1177/0954411911431516`.

[14] C. Klemt, D. Nolte, Z. Ding, *et al.*, “Anthropometric scaling of anatomical datasets for subject-specific musculoskeletal modelling of the shoulder,” *Annals of Biomedical Engineering*, vol. 47, pp. 924–936, 2019.

[15] A. Seth, M. Dong, R. Matias, and S. Delp, "Muscle contributions to upper-extremity movement and work from a musculoskeletal model of the human shoulder," *Frontiers in neurorobotics*, vol. 13, p. 90, 2019.

[16] I. Beck, I. Belli, L. Peternel, A. Seth, and J. M. Prendergast, "Real-time tendon strain estimation of rotator-cuff muscles during robotic-assisted rehabilitation," in *2023 IEEE-RAS 22nd International Conference on Humanoid Robots (Humanoids)*, IEEE, 2023, pp. 1–8.

[17] K. R. Holzbaur, W. M. Murray, and S. L. Delp, "A model of the upper extremity for simulating musculoskeletal surgery and analyzing neuromuscular control," *Annals of biomedical engineering*, vol. 33, pp. 829–840, 2005.

[18] M. D. Klein Breteler, C. W. Spoor, and F. C. Van der Helm, "Measuring muscle and joint geometry parameters of a shoulder for modeling purposes," *Journal of Biomechanics*, vol. 32, no. 11, pp. 1191–1197, 1999, ISSN: 0021-9290. [Online]. Available: https://www.sciencedirect.com/science/article/pii/S0021929099001220.

[19] F. van der Helm, "A finite element musculoskeletal model of the shoulder mechanism," *Journal of Biomechanics*, vol. 27, no. 5, pp. 551–569, 1994, ISSN: 0021-9290. [Online]. Available: https://www.sciencedirect.com/science/article/pii/0021929094900655.

[20] D. C. Ackland, P. Pak, M. Richardson, and M. G. Pandy, "Moment arms of the muscles crossing the anatomical shoulder," *Journal of anatomy*, vol. 213, no. 4, pp. 383–390, 2008.

[21] A. G. C. S. Carvalho, A. Seth, I. Belli, W. de Vries, and H. Veeger, "Muscle contributions to work during manual wheelchair propulsion," 2024. [Online]. Available: https://repository.tudelft.nl/record/uuid:89cdce79-f58d-45db-9bf0-0946113b81a1.

[22] I. Belli, S. Joshi, J. M. Prendergast, *et al.*, "Does enforcing glenohumeral joint stability matter? a new rapid muscle redundancy solver highlights the importance of non-superficial shoulder muscles," *PLOS ONE*, vol. 18, no. 11, pp. 1–19, Nov. 2023. [Online]. Available: https://doi.org/10.1371/journal.pone.0295003.

[23] K. A. Meszaros, M. E. Vidt, and C. R. Dickerson, "The effects of hand force variation on shoulder muscle activation during submaximal exertions," *International Journal of Occupational Safety and Ergonomics*, vol. 24, no. 1, pp. 100–110, 2017, PMID: 28007019. [Online]. Available: https://doi.org/10.1080/10803548.2016.1266805.

[24] C. van Andel, K. van Hutten, M. Eversdijk, D. Veeger, and J. Harlaar, "Recording scapular motion using an acromion marker cluster," *Gait & Posture*, vol. 29, no. 1, pp. 123–128, 2009, ISSN: 0966-6362. [Online]. Available: https://www.sciencedirect.com/science/article/pii/S0966636208002087.

[25] J. H. de Groot, L. A. Rozendaal, C. G. Meskers, and H. J. Arwert, "Isometric shoulder muscle activation patterns for 3-d planar forces: A methodology for musculo-skeletal model validation," *Clinical Biomechanics*, vol. 19, no. 8, pp. 790–800, 2004, ISSN: 0268-0033. [Online]. Available: https://www.sciencedirect.com/science/article/pii/S0268003304001226.

A

Latissimus dorsi changes

Table A.1: Geometry of the ellipsoid that is used as wrapping surface for the latissimus dorsi. The location is shown with respect to the thorax.

	X	Y	Z
Location centerpoint	-0.021999879226828334	-0.14670090464761937	0.069998363349739287
Radii	0.0840668	0.139952	0.0904834
Rotation	-0.17	-0.0383972	0.212232

Table A.2: Values used for the simmspline function used for the moving path point of the latissimus dorsi muscles. The first row shows the two planar elevation angles (in radians) where the position is given. The second to fourth row show the corresponding X, Y and Z location of the moving path point for these planar elevation angles, with respect to the thorax (in meters).

(a) Superior latissimus dorsi.

Planar elevation angle	0	3.14159
X	-0.08	0.02
Y	-0.085	-0.065
Z	0.13	0.175

(b) Middle latissimus dorsi,

Planar elevation angle	0	3.14159
X	-0.07	0.02
Y	-0.104	-0.084
Z	0.14	0.18

(c) Inferior latissimus dorsi.

Planar elevation angle	0	3.14159
X	-0.06	0.02
Y	-0.124	-0.104
Z	0.15	0.19

B
Muscle Activations

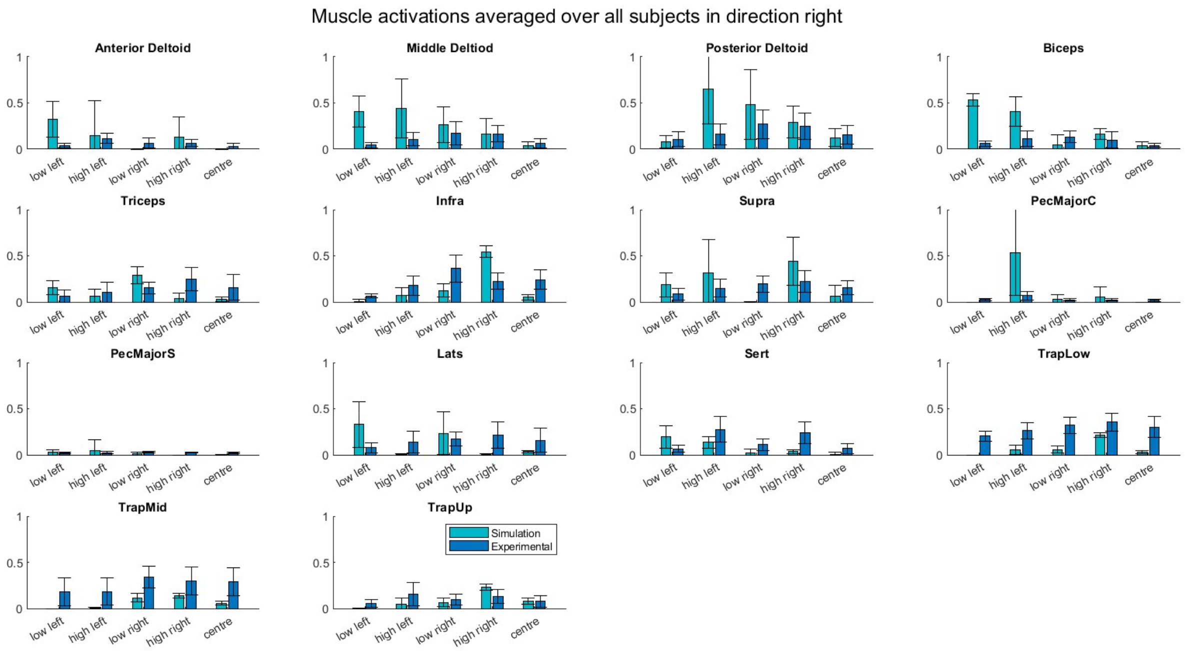

Figure B.1: Muscle activations of RMR solver compared to experimental data, pushing to the right. The activation levels are averaged over the seven subjects.

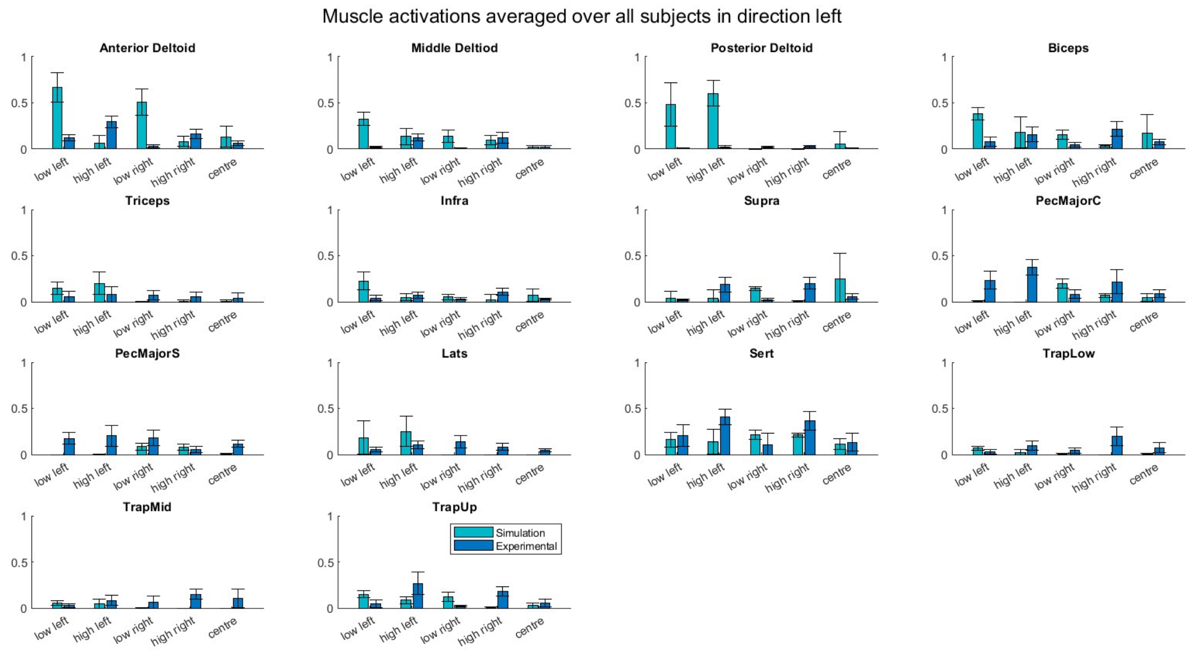

Figure B.2: Muscle activations of RMR solver compared to experimental data, pushing to the left. The activation levels are averaged over the seven subjects.

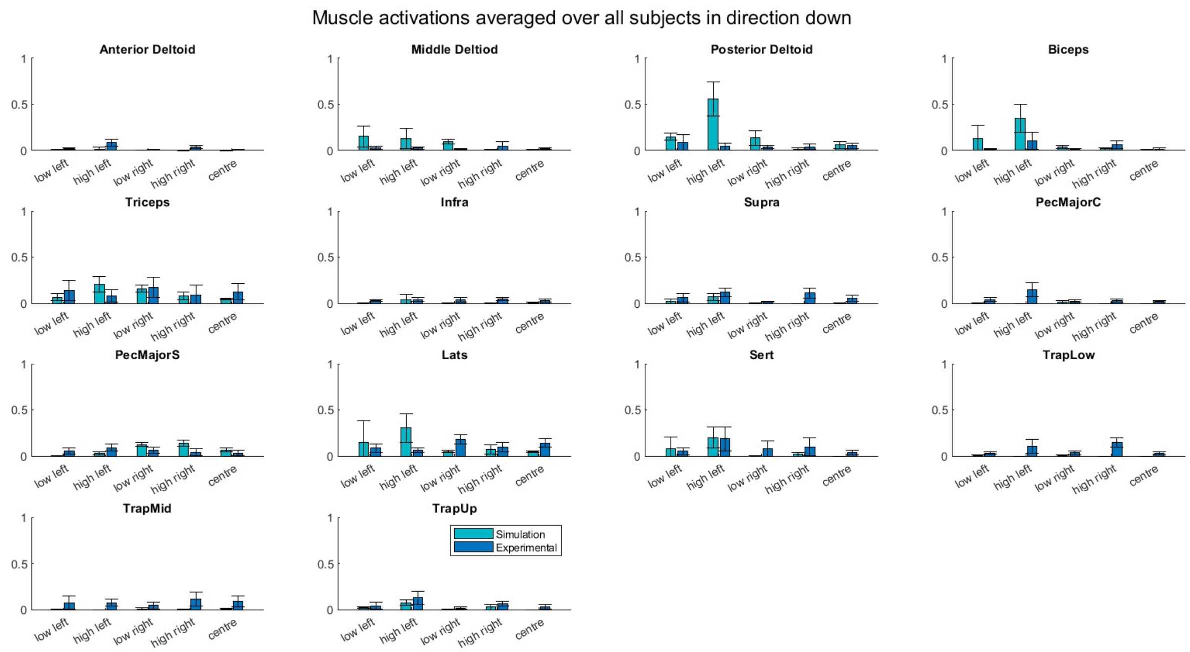

Figure B.3: Muscle activations of RMR solver compared to experimental data, pulling downwards. The activation levels are averaged over the seven subjects.

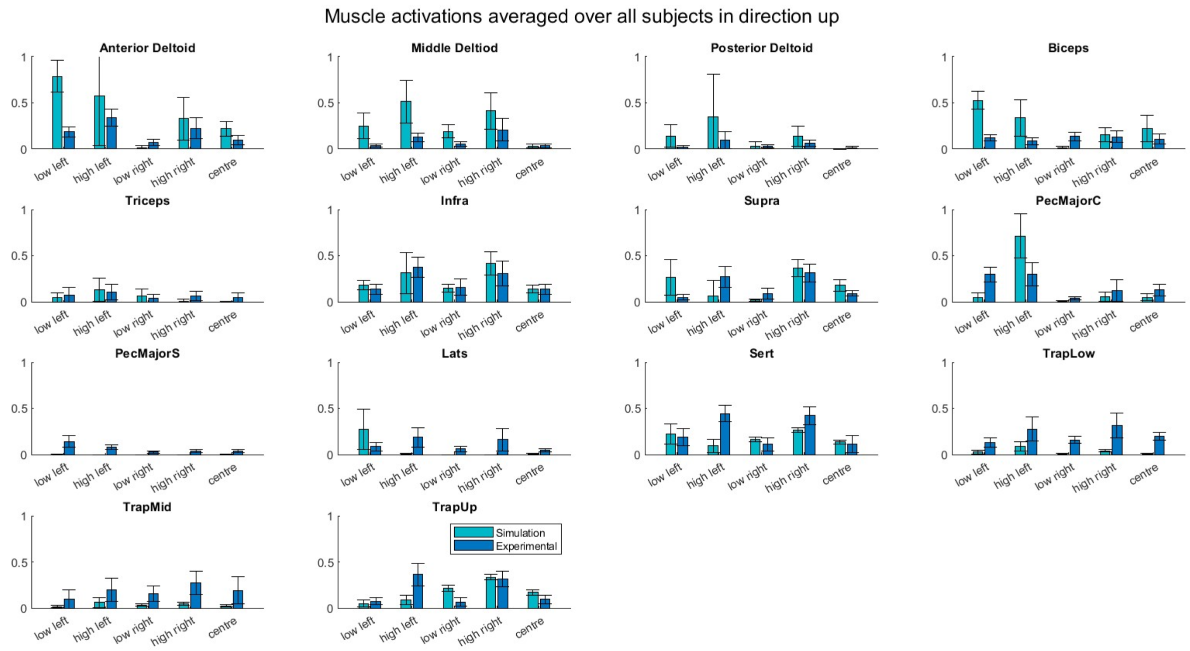

Figure B.4: Muscle activations of RMR solver compared to experimental data, pushing upwards. The activation levels are averaged over the seven subjects.

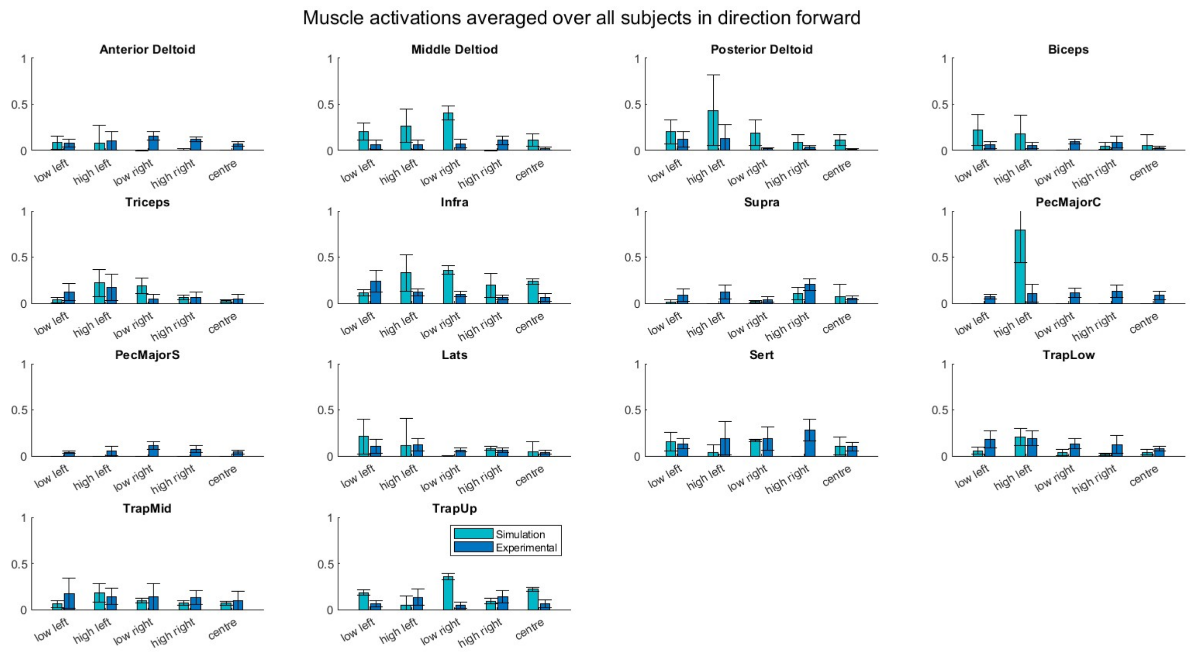

Figure B.5: Muscle activations of RMR solver compared to experimental data, pushing forwards. The activation levels are averaged over the seven subjects.

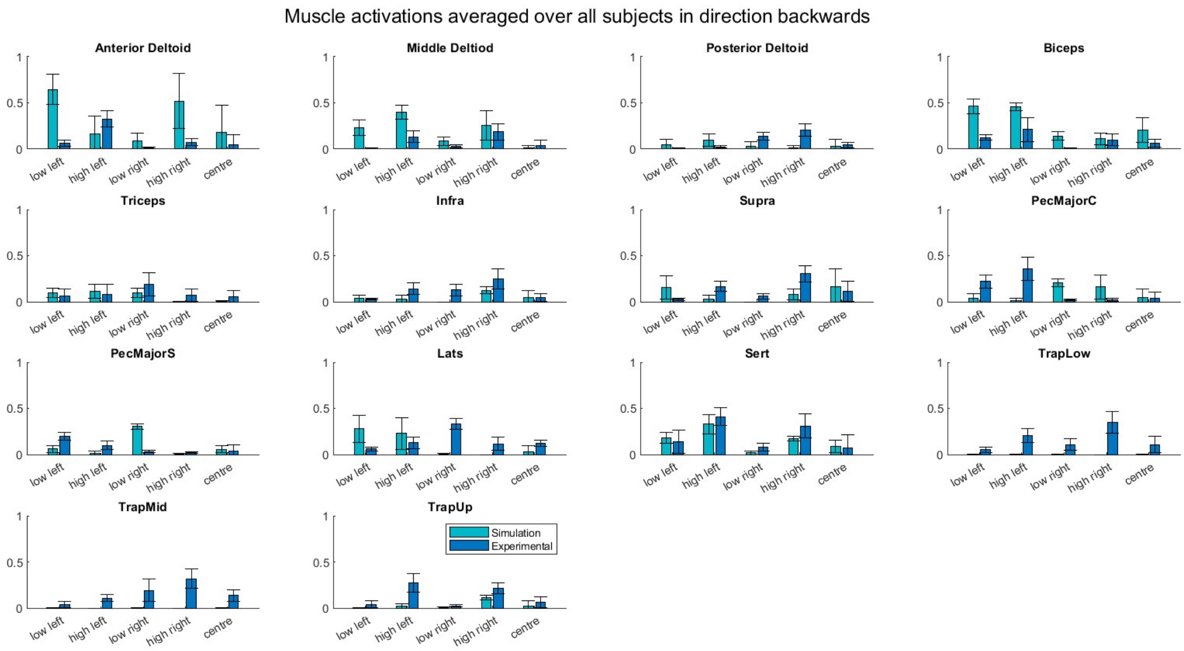

Figure B.6: Muscle activations of RMR solver compared to experimental data, pulling backwards. The activation levels are averaged over the seven subjects.